Electronic Supporting Information for the paper «Primary photochemical processes for ruthenium nitrosyl complex with nitrite and picoline ligands and photo dependent inhibition of endo III DNA glycosylase»

Artem A. Mikhailov[1,3], Vladislav A. Nichiporenko[1,2], Evgeni M. Glebov[1,2], Vjacheslav P. Grivin[1,2], Victor F. Plyusnin[1,2], Vadim V. Yanshole[1,4], Darya V. Khantakova[1,5], Daria V. Petrova[1,5], Gennadiy A. Kostin*[1,3], Inga R. Grin[1,5],

**** Corresponding author: kostin@niic.nsc.ru***

[1]Novosibirsk State University, 2 Pirogova str., Novosibirsk 630090, Russia

[2]Voevodsky Institute of Chemical Kinetics and Combustion SB RAS, 3 Institutskaya str., Novosibirsk 630090, Russia

[3]Nikolaev Institute of Inorganic Chemistry SB RAS, 3 Lavrenieva ave., *Novosibirsk 630090, Russia.*

[4]International Tomography Center SB RAS,

[5]SB RAS Institute of Chemical Biology and Fundamental Medicine, 8 Lavrentieva Ave., Novosibirsk 630090, Russia.

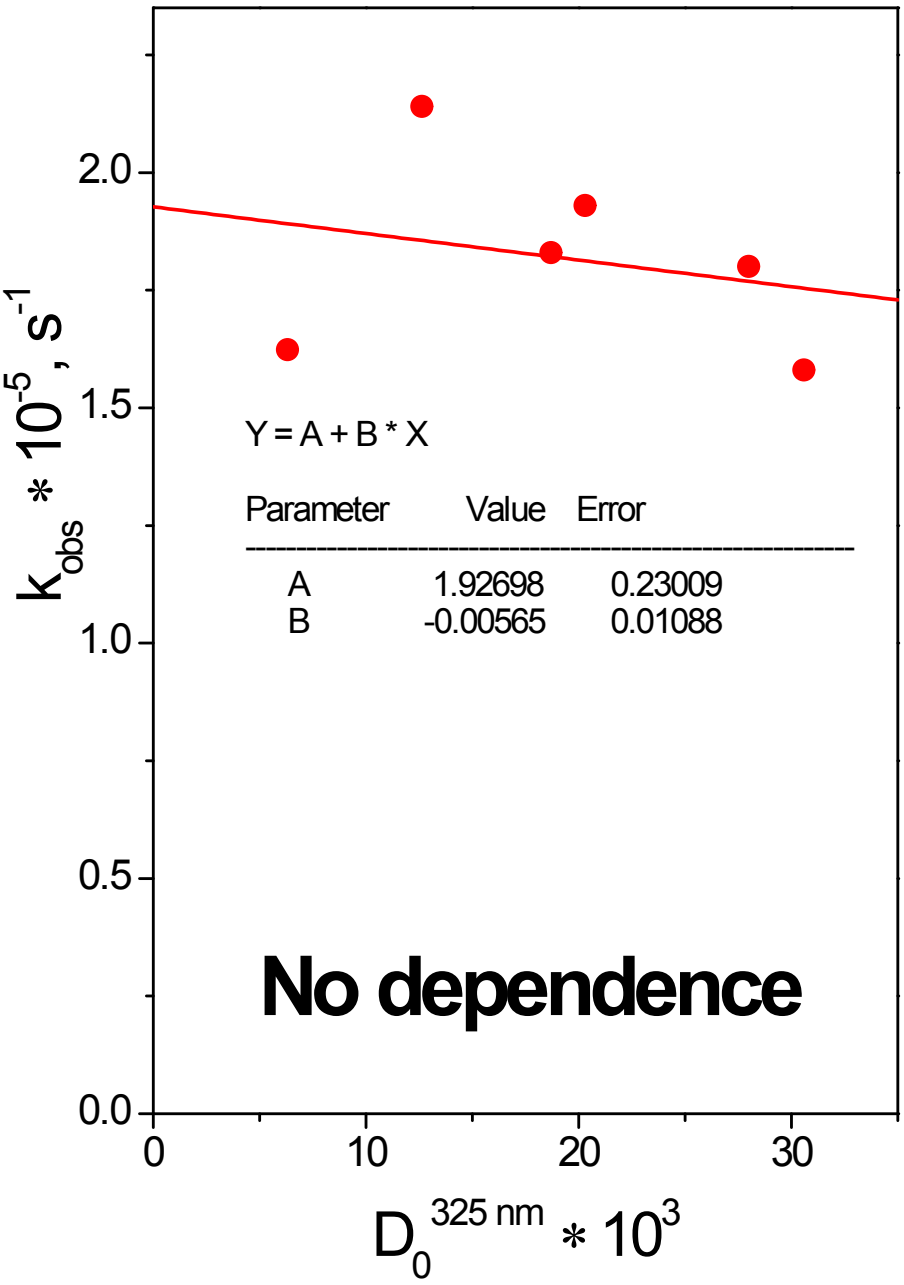

S1. Figure S1. Laser flash photolysis (266 nm) of $[Ru^{II}(NO)(NO_2)_2(Pic)_2(OH)]$ in CH3CN. 1 cm cell, O_2 - normal, $c_0 = 9.5\times10^{-5}$ M. Decay of intermediate absorption: k_1^{obs} vs. $(\Delta D)_0$. Absence of linear dependence means that the 2nd order processes are negligible. We have neither backward NO coordination nor Ru(III) disproportionation in the microsecond time domain.

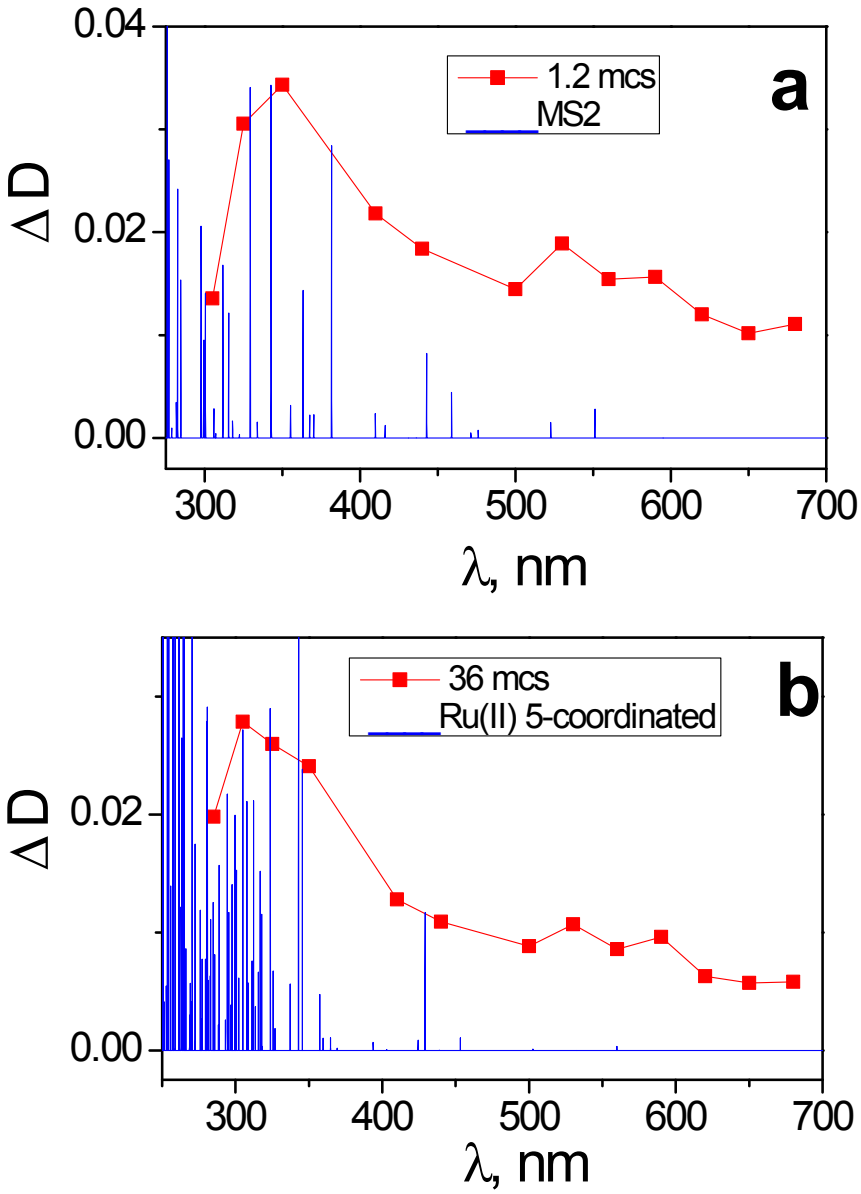

S2. Figure S2. Experimental and calculated intermediate absorption spectra obtained in the experiment on laser flash photolysis (266 nm) of $[Ru^{II}(NO)(NO_2)_2(Pic)_2(OH)]$ in CH_3CN. Comparison of the data shown in Figs. 4b and 6. **a** – initial spectrum of the intermediate absorption (curve 1 in Fig. 4b) and calculated spectrum of the MS2 intermediate. **b** – spectrum in 36 μs after the laser pulse (curve 1 in Fig. 4b) and calculated spectrum of the $[Ru^{III}(NO_2)_2(Pic)_2(OH)]$ intermediate.

S3. Lifetime of side-on isomer MS2 in the $[Ru^{II}(NO)(NO_2)_2(Pic)_2(OH)]$ powder as a function of temperature

IR spectra were recorded on the complex powder in KBr pellets on VERTEX 80vspectrometer. Photoisomerization GS-MS and reversed MS2-GS transformation was studied in cryostat cell at a temperature range 80 – 210 K. Irradiations were performed by 445 and 980 nm LED with 100 mW/cm2 optical power.

Nitrosyl ruthenium complexes can exist as three linkage isomers (Fig. S3-1). In the ground state (further – GS) the NO fragment is coordinated via the nitrogen atom. In addition, two bond isomers exist, namely MS1, in which the NO ligand is coordinated through the oxygen atom, and side-on (η^2-(NO)) or MS2 isomer at which nitrosyl ligand coordinated by both oxygen and nitrogen atoms to ruthenium. Bond isomers can be transferred to each other photochemically. MS1 to GS and MS2 to GS reactions can be driven by temperature as well (See Fig. S3-1).

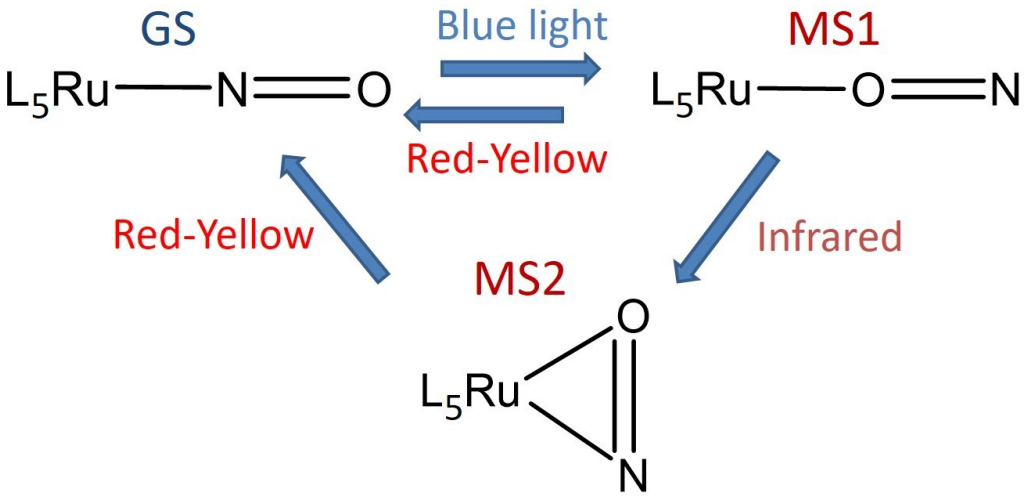

Figure S3-1. Bond isomers in nitrosyl ruthenium complexes.

In order to estimate the lifetime of the MS2 isomer at room temperature we determined the Arrhenius parameters for the MS2 to GS reaction from the low temperature experiments with the $[Ru^{II}(NO)(Pic)_2(NO_2)_2(OH)]$ powder. MS2 isomer was obtained by the subsequent 443 and 980 nm irradiation of the solid sample in KBr. The complex was incorporated in KBr pellet using the standard procedure of the solid samples preparation for the IR spectroscopy. The irradiation was performed at 80 K temperature. Fig. S3-2 demonstrates the characteristic IR bands of the GS, MS1 and MS2 isomers. After generation of MS2 at 80 K the sample was heated to higher temperature, and the kinetics of the MS2 decay was monitored via the intensity of the characteristic IR band of MS2 (Fig. S3-3, a). The experimental kinetic curves were fitted by means of the first-order kinetic law (Fig. S3-3, b). The values of activation energy and frequency factor of the MS2 decay extracted from the Arrhenius plot are $E_A = 33.3 \pm 4.6$ kJ/mole, and

Ln[k_0 (s^{-1})] = 20.6 ± 3.7 (Fig. S3-4). Estimation of the MS2 lifetime at 295 K taken using the best-fit values gives the value of 0.9 ms.

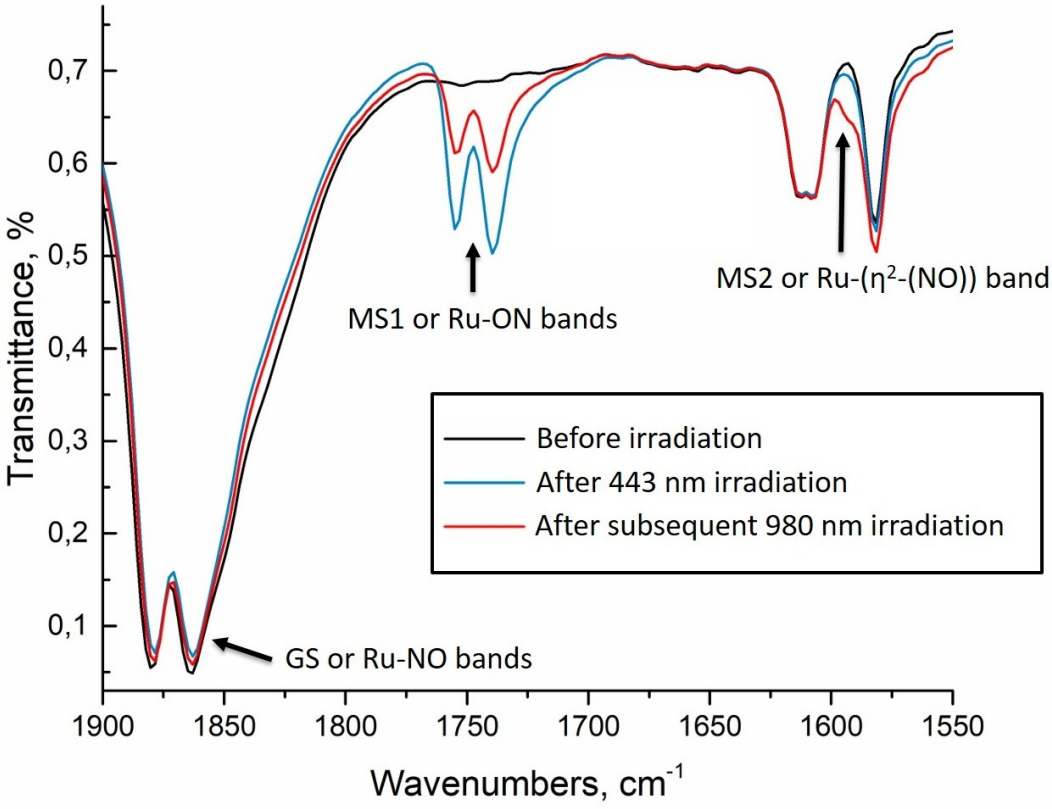

Figure S3-2. Characteristic fragment of the [Ru^{II}(NO)$(Pic)_2(NO_2)_2$(OH)] IR spectrum at 80 K before (black line), after 443 (blue line) and after subsequent 980 nm (red line) irradiation of the pellet (bands are doubled due to the two non-equivalent structures in the unit cell with the different surrounding near of the nitrosyl ligand).

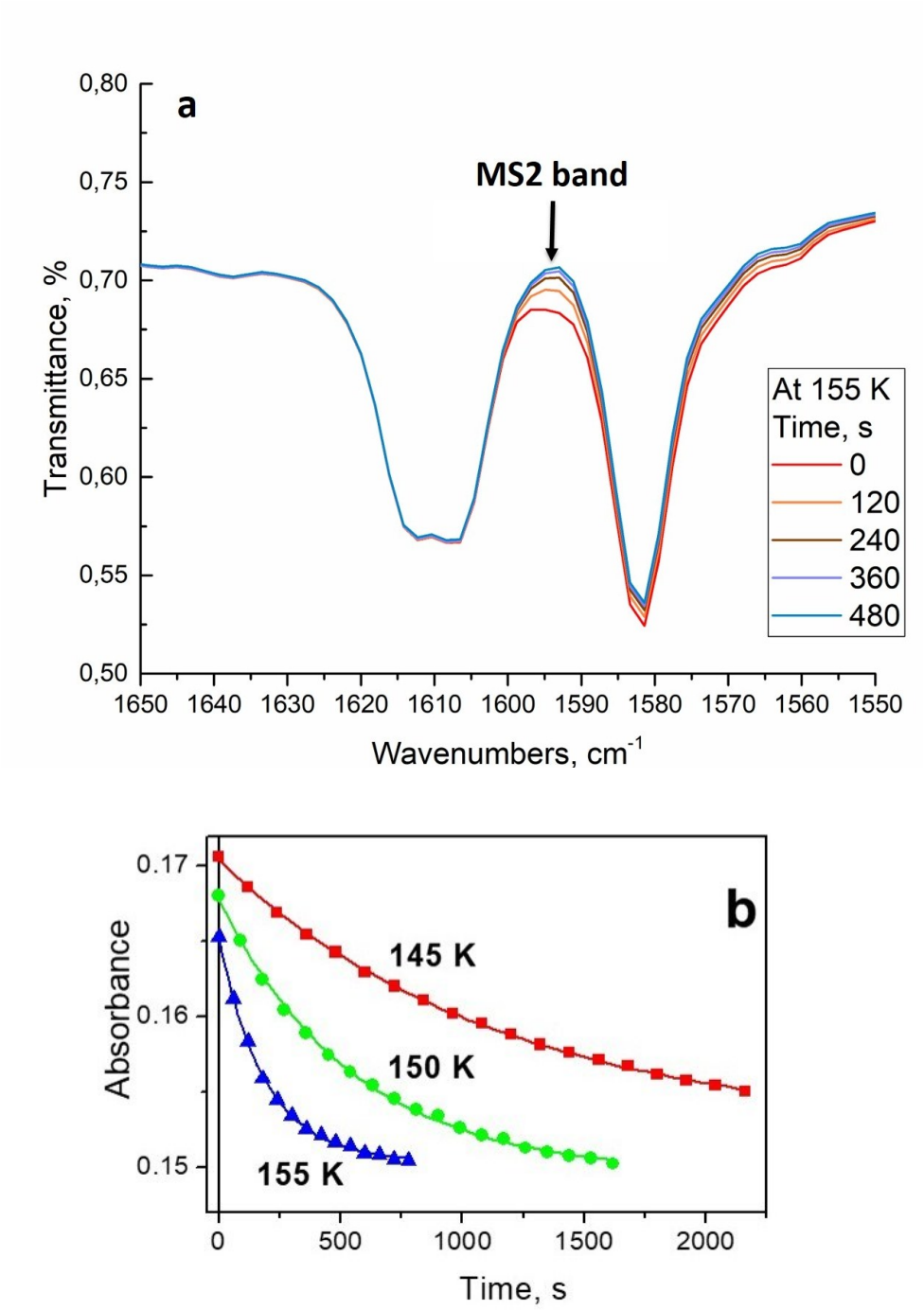

Figure S3-3. **a** - changes in the IR spectrum of $[Ru^{II}(NO)(NO_2)_2(Pic)_2(OH)]$ after sequential irradiation (443 and 980 nm at 80 K) due to thermal transition MS2 → GS at 155 K. **b** – kinetic curves of MS2 decay. Experimental points and 1-exponential fits.

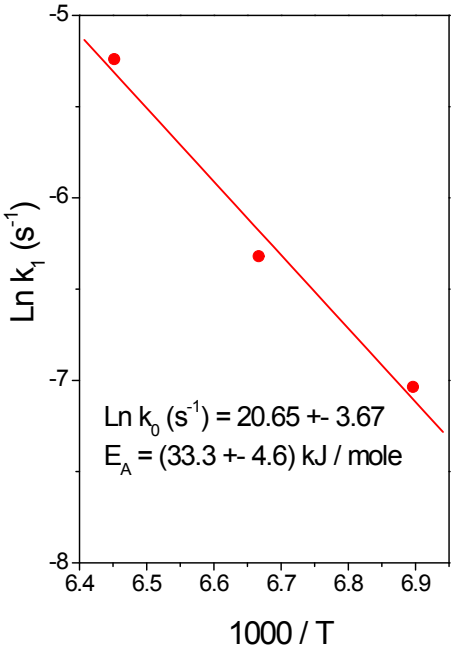

Figure S3-4. Arrhenius plot of the rate constant of the MS2 → GS reaction for the $[Ru^{II}(NO)(\beta\text{-Pic})_2(NO_2)_2(OH)]$ complex in the solid state. Treatment of the data of Fig. S3-2.

S4. DFT calculations of initial complex and potential intermediates.

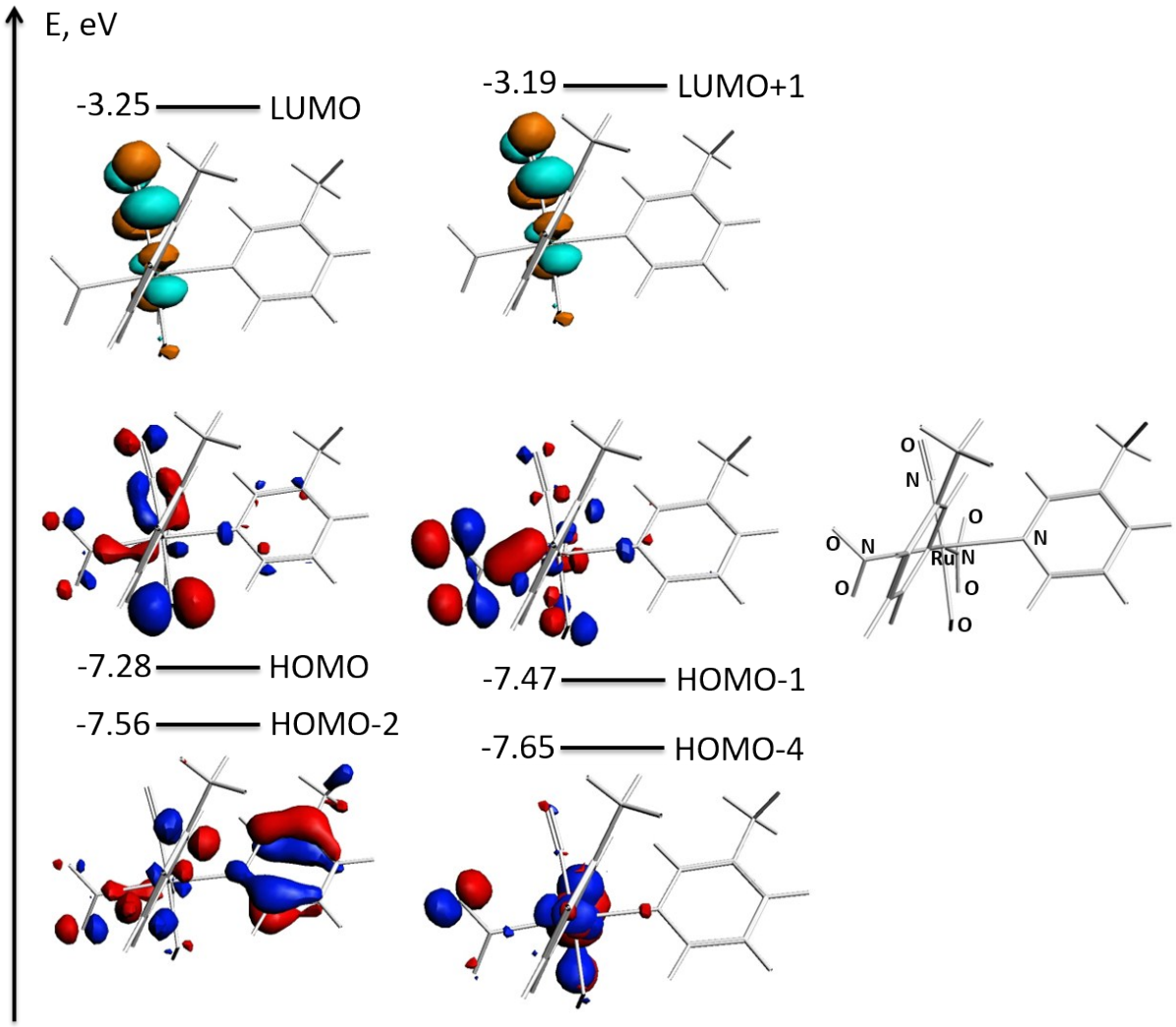

Figure S4. Chosen HOMO and LUMO orbitals of $[Ru^{II}NO(\beta\text{-}Pic)_2(NO_2)_2OH]$ complex.

Table S4-1. Coordinates of optimized $[Ru^{II}NO(\beta\text{-}Pic)_2(NO_2)_2OH]$ structure.

1.Ru	-1.722260	1.157672	-0.059381
2.H	4.274178	1.803302	-0.010744
3.O	-2.375126	3.968382	-0.542112
4.O	-4.561971	1.649581	0.496552
5.H	-1.587688	1.496747	5.946374
6.H	-1.627403	-1.165782	-0.678408
7.O	-1.595532	1.723834	-2.940275
8.N	0.445761	1.386229	-0.093904
9.C	1.209673	0.499794	0.563733
10.C	1.040564	2.412813	-0.733346
11.C	2.589644	0.625634	0.609352
12.C	2.415332	2.613493	-0.737979
13.C	3.197230	1.688577	-0.040390
14.H	0.690985	-0.319827	1.037647
15.H	0.391918	3.092124	-1.269512
16.C	3.024504	3.780041	-1.466543
17.H	3.170353	-0.107879	1.151853
18.N	-1.673614	1.295242	2.101599

19.C	-2.184374	0.299596	2.843044
20.C	-1.131464	2.360829	2.723675
21.C	-2.166707	0.346936	4.228731
22.C	-1.071931	2.488610	4.105121
23.C	-1.609245	1.444960	4.864372
24.H	-2.590280	-0.543292	2.304409
25.H	-0.727551	3.138743	2.089980
26.C	-0.455151	3.701784	4.745955
27.H	-2.587785	-0.474656	4.791704
28.N	-2.066564	2.889899	-0.312009
29.O	-1.738357	-0.390583	-2.557193
30.N	-3.820012	0.781692	0.004203
31.O	-4.287950	-0.269536	-0.440649
32.N	-1.688878	0.778263	-2.144811
33.O	-1.447272	-0.759762	0.188779
34.H	-1.192750	4.231437	5.351652
35.H	-0.066788	4.393134	3.999309
36.H	3.597239	4.405032	-0.778905
37.H	2.261057	4.397796	-1.937222
38.H	3.710776	3.432154	-2.240712
39.H	0.363654	3.412200	5.406953

Table S4-2. Coordinates of optimized [$Ru^{II}(\eta^2$-(NO))(β-Pic)$_2$(NO_2)$_2$OH] (MS2) structure.

1.Ru	-1.750050	1.157642	-0.068358
2.H	4.157875	2.095585	0.176982
3.O	-2.118361	3.183542	-0.856124
4.O	-4.589242	1.536550	-0.695106
5.H	-1.454787	1.328948	5.972413
6.H	-2.288484	-1.140750	0.356397
7.O	-1.074910	1.409147	-2.922389
8.N	0.368822	1.460521	-0.036575
9.C	1.130408	0.728153	0.794795
10.C	0.948728	2.405226	-0.798816
11.C	2.497631	0.930923	0.890190
12.C	2.309884	2.680818	-0.756980
13.C	3.090902	1.917274	0.113535
14.H	0.616333	-0.022280	1.375311
15.H	0.297125	2.945595	-1.470749
16.C	2.903889	3.757513	-1.621113
17.H	3.079919	0.320533	1.566723
18.N	-1.707049	1.278719	2.132428
19.C	-2.421578	0.412920	2.863887
20.C	-0.911853	2.164821	2.756558
21.C	-2.356946	0.411685	4.249876
22.C	-0.776780	2.225645	4.137068
23.C	-1.525875	1.319137	4.891111
24.H	-3.044966	-0.280871	2.321470
25.H	-0.356993	2.844118	2.123833
26.C	0.146719	3.223342	4.778716
27.H	-2.952691	-0.297829	4.807785
28.N	-2.173752	3.045148	0.310517

29.O	-2.165209	-0.408290	-2.527619
30.N	-3.815471	0.720399	-0.174569
31.O	-4.243489	-0.369054	0.248286
32.N	-1.650464	0.644075	-2.136740
33.O	-1.415374	-0.709515	0.343668
34.H	-0.406582	3.866852	5.466457
35.H	0.630290	3.850557	4.028950
36.H	3.372752	4.526450	-1.002297
37.H	2.140453	4.227803	-2.241511
38.H	3.676699	3.340548	-2.271041
39.H	0.919386	2.710635	5.356880

Table S4-3. Coordinates of optimized $[Ru^{III}(\beta\text{-Pic})_2(NO_2)_2OH]$ structure.

1.Ru	-1.689559	0.873707	-0.040308
2.H	4.130610	2.338294	0.084682
3.H	-0.019654	3.654274	5.284792
4.O	-3.577364	2.532319	-0.054798
5.H	-1.509394	1.401637	5.945454
6.H	-1.484629	-1.357702	-0.813639
7.O	-1.697698	1.748944	-2.798670
8.N	0.420332	1.335083	-0.052757
9.C	1.258650	0.710938	0.793712
10.C	0.896757	2.305801	-0.856232
11.C	2.599296	1.048430	0.860253
12.C	2.225364	2.712239	-0.843779
13.C	3.084873	2.058456	0.041496
14.H	0.835300	-0.067550	1.411502
15.H	0.184388	2.759758	-1.532843
16.C	2.709027	3.804565	-1.756130
17.H	3.246730	0.522902	1.548406
18.N	-1.649360	1.039305	2.114698
19.C	-1.930256	-0.009773	2.904578
20.C	-1.326281	2.215899	2.683729
21.C	-1.887295	0.091834	4.286607
22.C	-1.261454	2.407043	4.057699
23.C	-1.550196	1.305254	4.866901
24.H	-2.180581	-0.935636	2.407571
25.H	-1.108278	3.032910	2.006858
26.C	-0.895423	3.743893	4.639806
27.H	-2.116009	-0.775052	4.891106
28.H	3.496560	3.431729	-2.413346
29.O	-1.653906	-0.405181	-2.668196
30.N	-3.663287	1.275837	-0.009650
31.O	-4.730716	0.682507	0.049168
32.N	-1.686391	0.712666	-2.111549
33.O	-1.492779	-1.016035	0.103488
34.H	-1.713799	4.131054	5.249545
35.H	-0.675786	4.471594	3.859845
36.H	3.127725	4.629011	-1.176412
37.H	1.901455	4.194135	-2.373965

Table S4-4. Coordinates of optimized $[Ru^{II}(CH_3CN)(\beta\text{-}Pic)_2(NO_2)_2OH]^-$ structure.

1.Ru	-1.633554	1.195594	-0.013210
2.H	4.401134	1.350253	0.035529
3.H	3.957861	2.925149	-2.276621
4.O	-4.370775	1.715660	0.833334
5.H	-1.536745	1.331747	6.007064
6.H	-1.235408	-1.112794	-0.723380
7.O	-2.125618	1.800414	-2.845996
8.N	0.536079	1.282193	-0.019722
9.C	1.228575	0.362902	0.671896
10.C	1.225760	2.218608	-0.697703
11.C	2.616019	0.363252	0.714099
12.C	2.614403	2.293170	-0.719512
13.C	3.317360	1.334969	0.015683
14.H	0.630623	-0.387651	1.168671
15.H	0.633226	2.938066	-1.247177
16.C	3.320751	3.364933	-1.506541
17.H	3.132074	-0.395448	1.287981
18.N	-1.596105	1.286563	2.141313
19.C	-2.136643	0.280763	2.848399
20.C	-1.030220	2.302696	2.817417
21.C	-2.131991	0.268546	4.235799
22.C	-0.975770	2.375855	4.205662
23.C	-1.549118	1.323598	4.923070
24.H	-2.560584	-0.526701	2.269812
25.H	-0.603296	3.092558	2.214013
26.C	-0.323943	3.545267	4.894762
27.H	-2.581457	-0.562739	4.763049
28.H	0.507120	3.213615	5.520554
29.O	-1.068634	-0.049716	-2.570772
30.N	-3.678472	1.061183	0.008670
31.O	-4.293694	0.318382	-0.798761
32.N	-1.613839	0.968012	-2.059008
33.O	-1.469774	-0.868341	0.183719
34.H	-1.035240	4.059802	5.543858
35.H	0.060923	4.265595	4.173724
36.H	3.961544	3.965244	-0.857600
37.H	2.610254	4.031203	-1.994438
38.N	-1.775931	3.239462	-0.156232
39.C	-2.022432	5.825534	-0.352199
40.H	-1.454199	6.317870	0.436941
41.H	-3.072114	6.103787	-0.260574
42.H	-1.649560	6.159929	-1.320285
43.C	-1.883726	4.383499	-0.240165

Table S4-5. Coordinates of optimized $[Ru^{III}(CH_3CN)(\beta\text{-}Pic)_2(NO_2)_2OH]$ structure.

1.Ru	-1.609758	1.155038	-0.006297
2.H	4.405891	1.545160	0.047675
3.H	3.925436	2.882251	-2.386556
4.O	-4.349295	2.041753	0.471712

5.H	-1.574785	1.258600	6.016619
6.H	-1.677089	-1.082264	-0.782631
7.O	-1.409439	1.916609	-2.843121
8.N	0.559488	1.310829	-0.006153
9.C	1.281080	0.487132	0.772051
10.C	1.205458	2.206528	-0.775701
11.C	2.664389	0.548133	0.811326
12.C	2.589287	2.339144	-0.794960
13.C	3.324332	1.482106	0.026515
14.H	0.728922	-0.234167	1.355509
15.H	0.584177	2.830800	-1.402648
16.C	3.255412	3.363944	-1.672040
17.H	3.208295	-0.133069	1.451349
18.N	-1.590725	1.217956	2.158413
19.C	-2.144128	0.211190	2.854802
20.C	-1.032598	2.237031	2.838063
21.C	-2.153802	0.198746	4.241120
22.C	-0.995342	2.307444	4.225780
23.C	-1.576390	1.252446	4.932871
24.H	-2.570897	-0.595813	2.277871
25.H	-0.597699	3.026915	2.241570
26.C	-0.355617	3.476103	4.924750
27.H	-2.610384	-0.631847	4.761993
28.H	0.445082	3.139621	5.585766
29.O	-1.821135	-0.178931	-2.580021
30.N	-3.713422	1.077271	0.008889
31.O	-4.319475	0.086595	-0.429618
32.N	-1.621749	0.954084	-2.086860
33.O	-1.461601	-0.759820	0.114548
34.H	-1.086737	4.004554	5.539428
35.H	0.065058	4.183521	4.211477
36.H	3.855129	4.052216	-1.073700
37.H	2.522764	3.945253	-2.229868
38.N	-1.734224	3.267027	-0.124303
39.C	-2.046526	5.834134	-0.343689
40.H	-1.494431	6.345324	0.443368
41.H	-3.106735	6.068239	-0.255873
42.H	-1.683644	6.160404	-1.317286
43.C	-1.868069	4.403193	-0.217472

Table S4-6. Calculated DFT transitions, excitation energies and oscillator strength of $[Ru^{II}NO(\beta\text{-Pic})_2(NO_2)_2OH]$ complex. 107a – HOMO, 108a – LUMO.

Transition, occupancy	Energy, eV	λ, nm	*f*
107a -> 108a 0.7469 106a -> 108a 0.1026	2.71620	456	0.9961E-04
107a -> 109a 0.3925 103a -> 108a 0.2320 102a -> 109a 0.0663	3.24779	382	0.1190E-01
103a -> 108a 0.4037 107a -> 109a 0.1205 99a -> 108a 0.1067	3.51674	353	0.1257E-01

106a -> 109a 0.1051 104a -> 108a 0.0877				
105a -> 109a 0.5086 102a -> 109a 0.2120 104a -> 109a 0.0679	3.71571	334	0.2556E-02	
101a -> 109a 0.3257 102a -> 111a 0.1838	3.92430	316	0.3372E-02	
107a -> 111a 0.7620 106a -> 111a 0.0591	4.17452	297	0.1209E-01	
106a -> 111a 0.4750 106a -> 110a 0.0843	4.75971	260	0.2388	
102a -> 110a 0.1314 104a -> 110a 0.1279 105a -> 113a 0.0881 106a -> 114a 0.0618	5.12326	242	0.1956	
102a -> 112a 0.2010 102a -> 114a 0.1464 104a -> 113a 0.1236 104a -> 114a 0.0726	5.34094	232	0.1900	
104a -> 115a 0.2718 92a -> 109a 0.0972 105a -> 115a 0.0801	5.59444	222	0.1303	

Table S4-7. Calculated DFT transitions, excitation energies and oscillator strength of $[Ru^{II}(\eta^2\text{-}(NO))(\beta\text{-}Pic)_2(NO_2)_2OH]$ (MS2) complex. 107a – HOMO, 108a – LUMO.

Transition, occupancy	Energy, eV	λ, nm	*f*
103a -> 108a 0.4116 107a -> 108a 0.3081 106a -> 108a 0.0712	2.2495	551	0.1738E-02
107a -> 108a 0.4876 101a -> 108a 0.1944	2.70173	459	0.2755E-02
102a -> 108a 0.4270 105a -> 108a 0.2750 104a -> 108a 0.1934	2.79986	442	0.5626E-02
106a -> 109a 0.7151 107a -> 109a 0.1174	3.24907	382	0.1848E-01
102a -> 109a 0.4225 104a -> 109a 0.1542 105a -> 109a 0.1486 100a -> 109a 0.0699	3.61772	343	0.2239E-01
103a -> 109a 0.4447 104a -> 109a 0.1228 102a -> 109a 0.0733	3.76546	329	0.2998E-01
96a -> 108a 0.4930 100a -> 109a 0.1753 97a -> 108a 0.1348	3.97814	312	0.1068E-01
101a -> 110a 0.2115 95a -> 108a 0.1967 105a -> 110a 0.0811 107a -> 110a 0.0810	4.16515	298	0.2051E-01

106a -> 110a 0.2171 107a -> 110a 0.1521 106a -> 111a 0.1195 107a -> 111a 0.1166 102a -> 110a 0.1035	4.67142	265	0.1150
100a -> 110a 0.3005 102a -> 112a 0.1001 101a -> 112a 0.0918	5.20011	238	0.1630
105a -> 115a 0.1877 104a -> 115a 0.1162 103a -> 115a 0.0894 102a -> 115a 0.0831	5.73511	216	0.3002

Table S4-8. Calculated DFT transitions, excitation energies and oscillator strength of [Ru^{III}(β-Pic)$_2$(NO_2)$_2$OH] complex. 99a – HOMO, 100a – LUMO for Beta and 100a – HOMO, 101a – LUMO for Alpha spin state.

Transition, occupancy	Energy, eV	λ, nm	*f*
Beta 99a -> 100a 0.9447	0.94796	1308	0.8037E-04
Beta 98a -> 100a 0.8715	1.44608	857	0.5091E-03
Beta 96a -> 100a 0.8704	2.73582	453	0.3093E-03
Alpha 99a -> 101a 0.4481 Beta 99a -> 101a 0.3694	2.88921	429	0.4447E-02
Beta 98a -> 101a 0.3645 Alpha 98a -> 101a 0.2880 Alpha 95a -> 101a 0.1892	3.46867	357	0.1214E-02
Beta 92a -> 100a 0.4343 Beta 90a -> 100a 0.0858 Beta 91a -> 100a 0.0742	3.61567	343	0.1212E-01
Beta 98a -> 102a 0.1931 Beta 90a -> 100a 0.1806 Beta 94a -> 101a 0.1444 Alpha 94a -> 101a 0.1031	4.06589	305	0.1198E-01
Alpha 100a -> 104a 0.1600 Alpha 95a -> 101a 0.1239 Beta 99a -> 104a 0.0864 Beta 88a -> 100a 0.0834 Alpha 98a -> 101a 0.0768	4.41458	281	0.1111E-01
Alpha 98a -> 103a 0.2085 Beta 96a -> 102a 0.1832 Beta 98a -> 103a 0.1164 Alpha 95a -> 103a 0.0946	4.74121	262	0.4528E-01
Beta 97a -> 103a 0.3486 Beta 99a -> 106a 0.0926 Alpha 98a -> 103a 0.0862	5.09955	243	0.3977E-01
Alpha 98a -> 105a 0.1175 Beta 96a -> 105a 0.1119 Beta 97a -> 104a 0.0900	5.28118	235	0.2277E-01

Table S4-9. Calculated DFT transitions, excitation energies and oscillator strength of $[Ru^{II}(CH_3CN)(\beta\text{-Pic})_2(NO_2)_2OH]^-$ complex. 111a – HOMO, 112a – LUMO.

Transition, occupancy	Energy, eV	λ, nm	*f*
111a -> 113a 0.6277 111a -> 112a 0.1780 111a -> 114a 0.1619	2.82798	438	0.1399E-01
110a -> 112a 0.8210 110a -> 113a 0.1358	3.27119	379	0.6048E-01
109a -> 112a 0.3220 109a -> 113a 0.2290 111a -> 119a 0.1633 109a -> 114a 0.0825	3.58203	346	0.1408
111a -> 116a 0.3083 109a -> 114a 0.2600 109a -> 113a 0.2002 109a -> 115a 0.0768	3.64079	341	0.1601
109a -> 115a 0.2156 111a -> 120a 0.1407 109a -> 120a 0.0632	4.15204	299	0.2559E-01
111a -> 123a 0.1705 107a -> 112a 0.0947 110a -> 122a 0.0886 111a -> 120a 0.0842 111a -> 121a 0.0776	4.75200	261	0.3213E-01
105a -> 112a 0.1502 110a -> 122a 0.1442 105a -> 113a 0.1284 105a -> 114a 0.0786	5.20491	238	0.1828
109a -> 122a 0.1926 110a -> 122a 0.0991 107a -> 116a 0.0898	5.48456	226	0.1760
107a -> 120a 0.1761 108a -> 119a 0.1444 108a -> 118a 0.1104 108a -> 120a 0.1037 99a -> 114a 0.0855	6.10857	203	0.1382

Table S4-10. Calculated DFT transitions, excitation energies and oscillator strength of $[Ru^{III}(CH_3CN)(\beta\text{-Pic})_2(NO_2)_2OH]$ complex. 110a – HOMO, 111a – LUMO for Beta and 111a – HOMO, 112a – LUMO for Alpha spin state.

Transition, occupancy	Energy, eV	λ, nm	*f*
Beta 110a -> 111a 0.9598	0.65872	1882	0.4729E-04
Beta 109a -> 111a 0.8998	1.09711	1130	0.2882E-03
Beta 108a -> 111a 0.8800 Beta 107a -> 111a 0.0814	2.30433	538	0.2822E-03
Beta 104a -> 111a 0.5266 Beta 106a -> 111a 0.1916	2.75576	450	0.6432E-02

Beta 105a -> 111a 0.1624			
Beta 102a -> 111a 0.7799	3.27567	379	0.1626E-01
Beta 99a -> 111a 0.2538 Beta 102a -> 111a 0.0685	3.73655	332	0.7530E-02
Beta 110a -> 114a 0.1881 Alpha 111a -> 116a 0.1126 Beta 110a -> 116a 0.0955	4.00825	309	0.3735E-02
Beta 110a -> 115a 0.2633 Beta 110a -> 112a 0.1881 Beta 110a -> 114a 0.1368 Beta 109a -> 115a 0.0795	4.32113	287	0.1063E-01
Alpha 109a -> 113a 0.3047 Beta 109a -> 113a 0.0933 Alpha 110a -> 114a 0.0659	4.72240	263	0.3511E-01
Beta 108a -> 115a 0.2185 Beta 106a -> 113a 0.1118 Beta 106a -> 112a 0.0985	5.15072	241	0.2766E-01
Alpha 104a -> 116a 0.1501 Alpha106a -> 115a 0.1127 Alpha 108a -> 118a 0.0684	5.42883	228	0.6813E-02

Table S4-11. Chosen experimental (SCXRD) and calculated (DFT) bond distances of $[Ru^{II}NO(\beta\text{-Pic})_2(NO_2)_2OH]$ complex.

Method	Bond length, Å				
	Ru-N(NO)	Ru-N(β-Pic)	Ru-N(NO_2)	Ru-OH	N=O
SCXRD	1.771	2.122; 2,129	2.065; 2,085	1.915	1.157
	1.750	2.138; 2,133	2.075; 2,067	1.925	1.172
DFT	1,784	2,180; 2,166	2,120; 2,132	1,953	1,145

S5. Biochemical studies.

Table S5-1. Oligonucleotide sequences

name	sequence	X (modification)
FAM-23U	5′-(5,6-**FAM**)CTCTCCCTTC**X**CTCCTTTCCTCT-3′	uracil
23U	5′-CTCTCCCTTC**X**CTCCTTTCCTCT-3′	uracil
23hoU	5'-CTCTCCCTTC**X**CTCCTTTCCTCT-3'	5-hydroxyuracil
23DHU	5'-CTCTCCCTTC**X**CTCCTTTCCTCT-3'	dihydrouracil
Compl 1	5′-AGAGGAAAGGAGGGAAGGGAGAG-3′	
20mC	5′-GAGTGAGA**X**GTCAAGTTGGG-3'	5-methylcytosine
Compl 2	5′-CCCAACTTGACGTCTCACTC-3′	

Table S5-2. Double-stranded DNA substrates

name	Labeled strand	Complementary strand
{FAM-23U}→{FAM-23AP}§	FAM-23U	Compl 1
{*23U}→{*23AP}§	*23U	Compl 1
{*23hoU}	*23hoU	Compl 1
{*23DHU}	*23DHU	Compl 1
{*23mC}	*20mC	Compl 2

* Radioactive-labeled strand; § duplex with uracil was treated by Uracil-DNA glycosylase to generate AP-site.

Figure S5-1. ***E. coli*** **Endo III purification.** Lines 1 and 2, precipitate and lysate after sonication; line 3, 520–730 mM NaCl protein fraction after 5 mL HiTrap SP Sepharose FF column (1); line 4, 5, 920–1000 mM NaCl protein fraction after 1 mL HiTrap Heparin HP column (2) in gels with markers M1 and M2; line 6, *E. coli* Endo III (23 kDa) after SOURCE 15 PHE (phenyl) column and Amicon Ultra centrifugation.

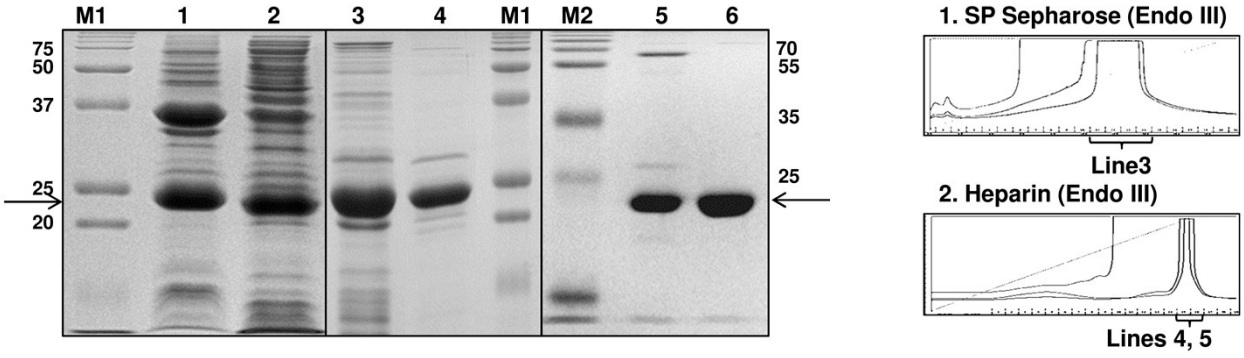

Figure S5-2. Enzyme-concentration dependence. The reaction mixture (20 µl) contained duplex substrate with AP-site (A) or 5-hoU (B) in the reaction buffer and 0 – 150 nM Endo III. After 20 min at 37°C reaction was stopped by mixing with an equal volume of the loading buffer (80% formamide, 20 mM Na–EDTA, 0.1% xylene cyanol, 0.1% bromophenol blue) and heated for 2 min at 95°C. The incised product (P) was separated from the substrate (S) on 20% denaturing PAGE (8 M urea).

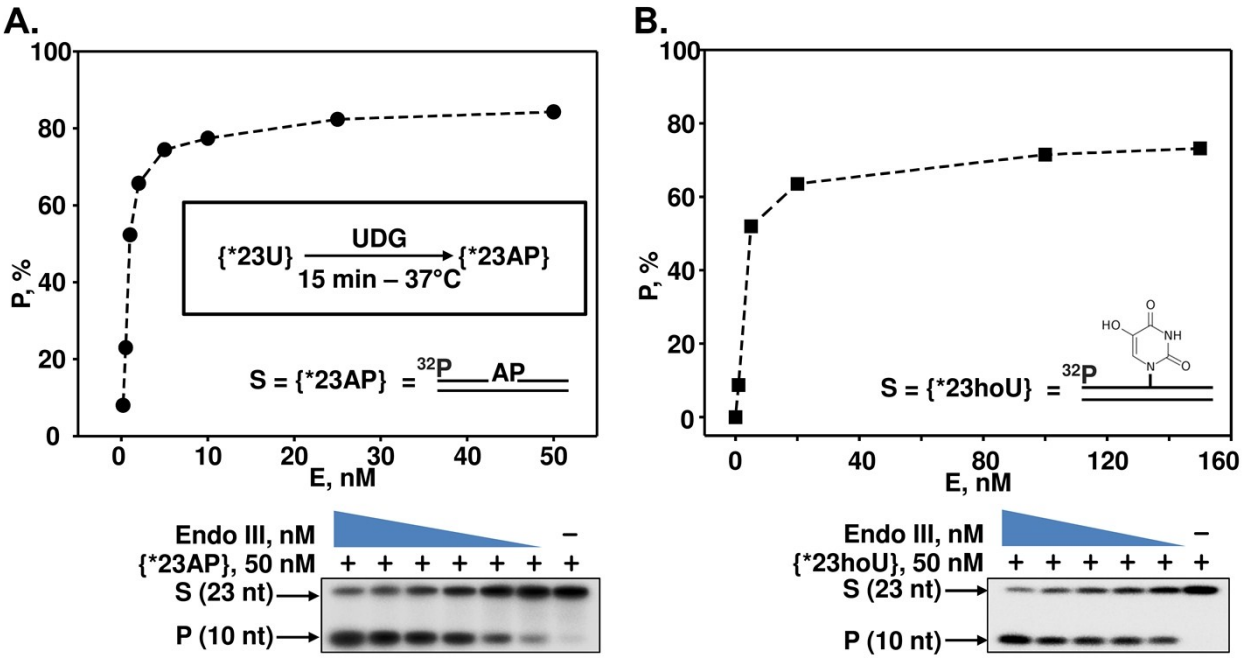

Figure S5-3. **Exposure time (A) and [Ru(NO)(β-Pic)$_2$(NO$_2$)$_2$(OH)]-concentration (B) dependences for inhibiting DNA-glycosylase activity of Endo III**. A) The reaction mixture 1 (20 µl) contained 100 nM Endo III, 10 mM ruthenium nitrosyl complex [Ru(NO)(β-Pic)$_2$(NO$_2$)$_2$(OH)] ([RuNOL$_5$]) and was irradiated at 445 nm for 0 – 30 min on ice. B) The reaction mixture 1 (20 µl) contained Endo III, 0 – 5 mM [RuNOL$_5$] and was irradiated at 445 nm for 5 min on ice. After irradiation 10 µl of the reaction mixture 1 was added to 10 µl 100 nM DNA substrate with 5-hoU and incubated 20 min at 37°C. Reaction was stopped by mixing with an equal volume of the loading buffer (80% formamide, 20 mM Na–EDTA, 0.1% xylene cyanol, 0.1% bromophenol blue) and heated for 2 min at 95°C. The incised product (P) was separated from the substrate (S) on 20% denaturing PAGE (8 M urea). The inhibition efficiency of the activity Endo III (PI) was calculated by subtracting nonspecific background activity in negative control experiments (Kneg) and normalization to the maximum of DNA glycosylase activity (Kpos), according to Equation: PI = 100% – [(P,% – Kneg)/(Kpos – Kneg)×100%].

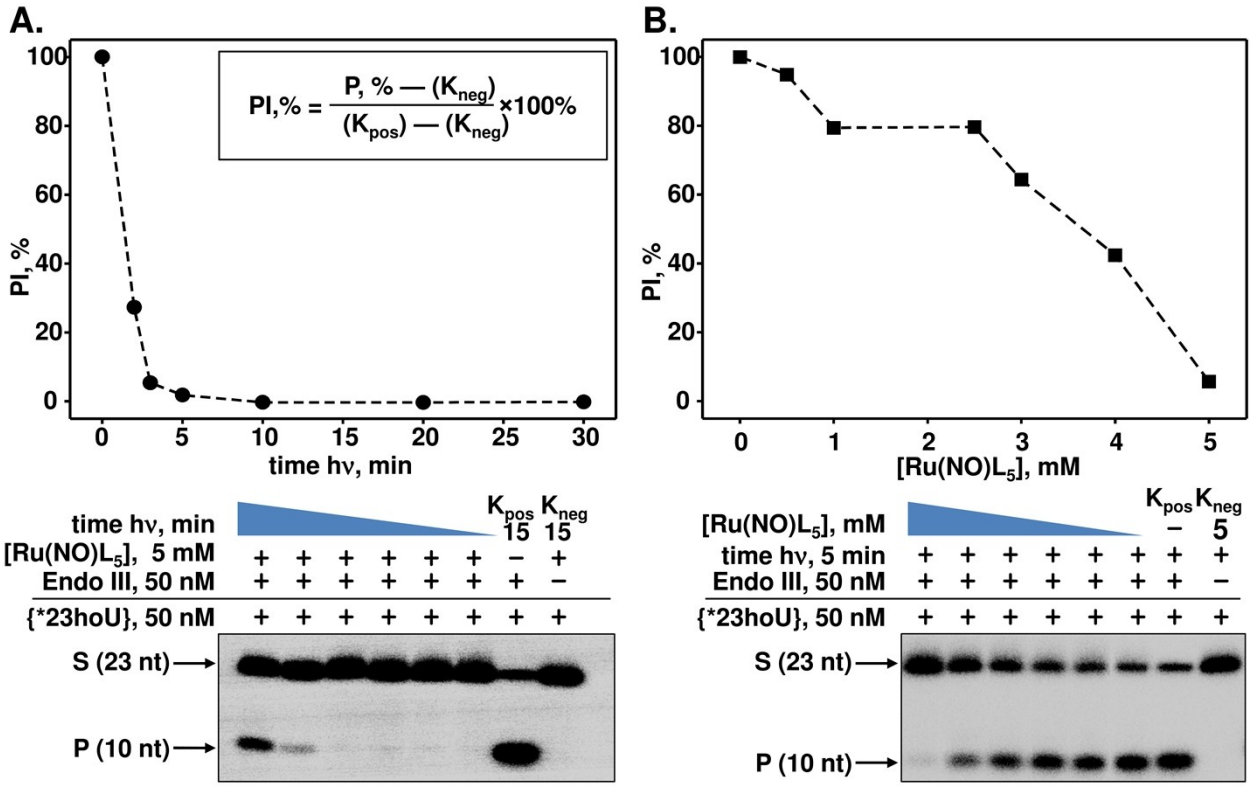

Figure S5-4. Inhibiting DNA-glycosylase activity of Endo III on DNA substrate with dihydrouracil by photolisys products of $[Ru(NO)(\beta\text{-}Pic)_2(NO_2)_2(OH)]$ complex.

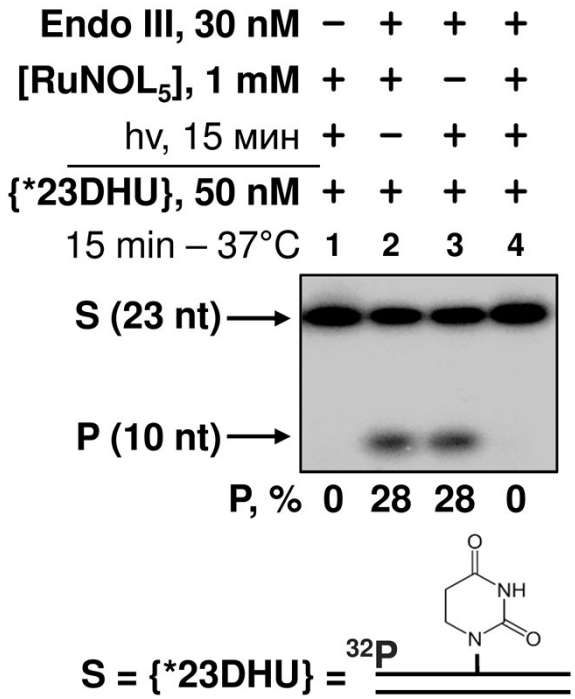

Figure S5-5. **UV/vis spectroscopy data.** The absorption data were acquired with the reference of buffer solution (20 mM sodium phosphate, pH 7.4, 400 mM NaCl, 30 μM Na-EDTA, 30 μM DTT, 16% glycerol, 80 μg/ml BSA, 1.5% DMSO). (A) The samples contained 50 μM Endo III with 50 μM [Ru(NO)(β-Pic)$_2$(NO$_2$)$_2$(OH)] complex and were exposure by laser running at 445 nm with 100 mW cm^{-2} power on ice for different time: 1 – 0 min, 2 – 1 min, 3 – 5 min, 4 – 9 min, 5 – 15 min, 6 – 20 min. (B) The samples contained 50 μM Endo III with 50 μM (2, 5), 100 μM (3, 6) or 150 μM (4,7) [Ru(NO)(β-Pic)$_2$(NO$_2$)$_2$(OH)] complex. The samples 1 is Endo III without [Ru(NO)(β-Pic)$_2$(NO$_2$)$_2$(OH)] complex. The samples 4, 5 and 6 were exposure by laser running at 445 nm with 100 mW cm^{-2} power on ice for 15 min.

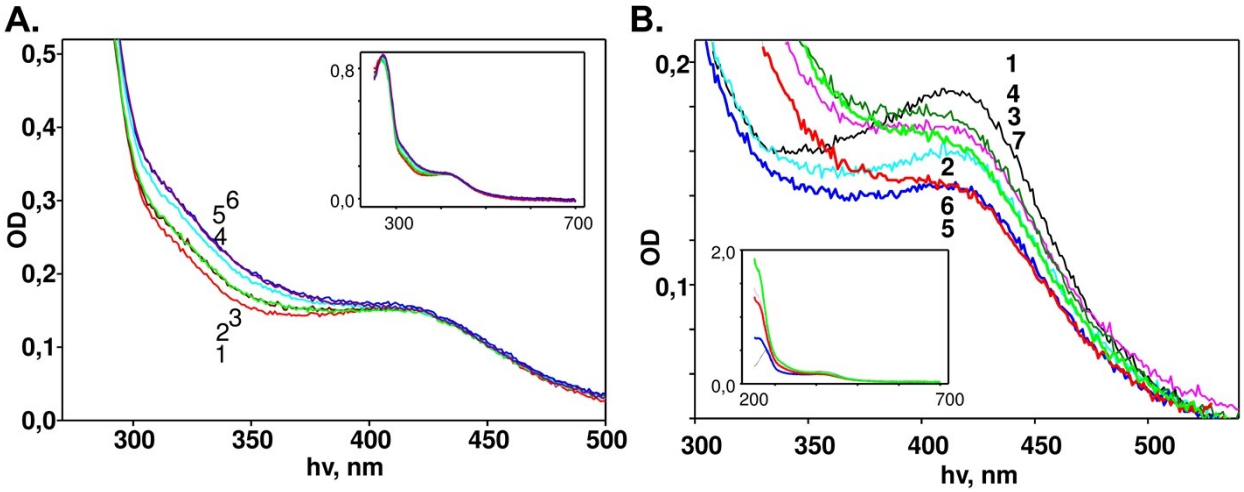

Figure S5-6. AP-lyase activity of *E. coli* Endo III on AP-substrate labeled FAM (5' 6-Fluorescein). Line 1: AP-substrate with Endo III after 15 min irradiation in ice and AP-lyase reaction (20 min at 37°C); line 2: AP-substrate and [Ru(NO)(β-Pic)$_2$(NO$_2$)$_2$(OH)] were irradiated 15 min in ice followed by adding the Endo III (20 min at 37°C); line 3: AP-substrate with Endo III and [Ru(NO)(β-Pic)$_2$(NO$_2$)$_2$(OH)] without irradiation (20 min at 37°C); line 4: AP-substrate with Endo III and [Ru(NO)(β-Pic)$_2$(NO$_2$)$_2$(OH)] after irradiation 15 min in ice and AP-lyase reaction (20 min at 37°C); line 5: AP-substrate with [Ru(NO)(β-Pic)$_2$(NO$_2$)$_2$(OH)]; line 6: AP-substrate. The incised product (P) was separated on a denaturing polyacrylamide electrophoresis gel (20%), subjected to the PhosphoImaging analysis and calculated as a ratio (P, %) lower band (P) to the total band intensity (S+P).

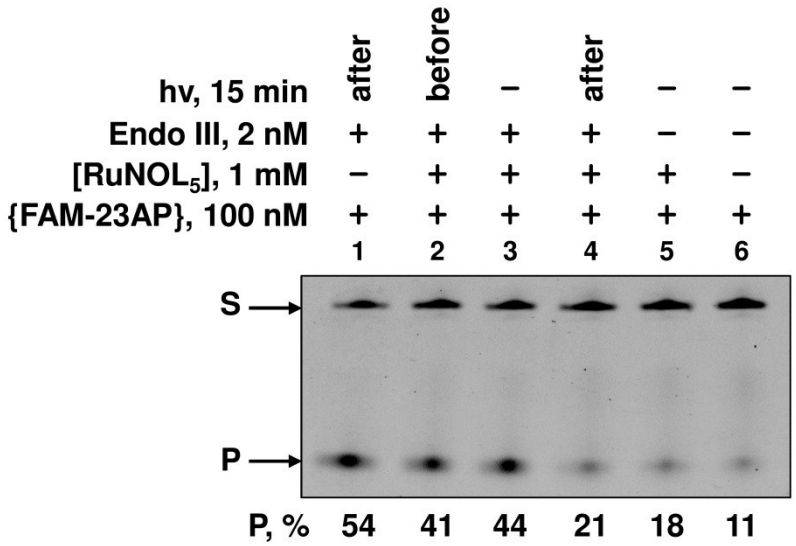

S6. HPLC-MC investigation of stationary photolysys products.

The rising peak at RT 1.30 min (Fig. S6-1) is formed by three main ruthenium-containing species (See summary Table below) and $[(\beta\text{-Pic}) + H^+]^+$ cation. The MS isotopic patterns could be attributed to the species formed during the ESI of the $[Ru^{II}(CH_3CN)(\beta\text{-Pic})_2(NO_2)_2(OH)]^-$ complex. This is supported by the detection of free β-picoline in the mass spectrum of this peak. Note that the species with *m/z* = 282.989 is the Ru^I complex. The reduction of Ru^{II} to Ru^I seems to occur in the course of the electrospray ionization.
Two peaks with RT 4.91 and 5.29 min give rise to the same Ru^{II} and Ru^I species. They could belong to $[Ru^{II}(\beta\text{-Pic})_2(NO_2)_2(H_2O)(OH)]^-$ and $[Ru^{II}(\beta\text{-Pic})_2(NO_2)_2(H_2O)_2]$ complexes (the second complex is the result of protonation of the first one). This identification is supported by our preliminary results on the $[Ru^{II}(NO)(\beta\text{-Pic})_2(NO_2)_2(OH)]$ photolysis in aqueous solutions, which gives rise to the same species (note that the neat acetonitrile contains ca. 10^{-2} M of water, which makes possible the formation of minor photolysis products containing water molecules).

Summary of HPLC – MS studies.

HPLC-MS study		
RT – 1.3 min (↑)		
94.065	$(\beta\text{-Pic})^0 \cdot H^+$	94.065
282.989	$[Ru^I(\beta\text{-Pic})(NO_2)(CH_3CN)]^0 \cdot H^+$	282.989
328.981	$[Ru^{II}(\beta\text{-Pic})(NO_2)_2(CH_3CN)]^0 \cdot H^+$	328.982
381.013	$[Ru^{II}(\beta\text{-Pic})_2(NO_2)_2]^0 \cdot H^+$	381.013
RT – 4.92 and 5.31 min (↑)		
335.020	$[Ru^I(\beta\text{-Pic})_2(NO_2)]^0 \cdot H^+$	335.020
381.013	$[Ru^{II}(\beta\text{-Pic})_2(NO_2)_2]^0 \cdot H^+$	381.013
RT – 6.25 and 6.33 min		
335.021	$[Ru^I(\beta\text{-Pic})_2(NO_2)]^0 \cdot H^+$	335.020
381.013	$[Ru^{II}(\beta\text{-Pic})_2(NO_2)_2]^0 \cdot H^+$	381.013
474.072	$[Ru^{II}(\beta\text{-Pic})_3(NO_2)_2]^0 \cdot H^+$	474.071
RT – 6.90 (↓), 7.15 and 7.59 min (↓)		
320.009	$[Ru^{II}(\beta\text{-Pic})_2(NO_3)]^+$	320.009
334.013	$[Ru^I(NO)(\beta\text{-Pic})_2(NO_2)]^+$	334.012
350.008	$[Ru^I(NO)(\beta\text{-Pic})_2(NO_3)]^+$	350.007
364.011	$[Ru^0(NO^+)_2(\beta\text{-Pic})_2(NO_2^-)]^+$	364.010
380.007	$[Ru^{II}(NO)(\beta\text{-Pic})_2(NO_2)_2]^+$	380.005
410.004	$[Ru^I(NO^+)_2(\beta\text{-Pic})_2(NO_2^-)_2]^+$	410.003
428.013	$[Ru^{II}(NO)(\beta\text{-Pic})_2(NO_2)_2(OH)]^0 \cdot H^+$	428.014
449.997	$[Ru^{II}(NO)(\beta\text{-Pic})_2(NO_2)_2(OH)]^0 \cdot Na^+$	449.996

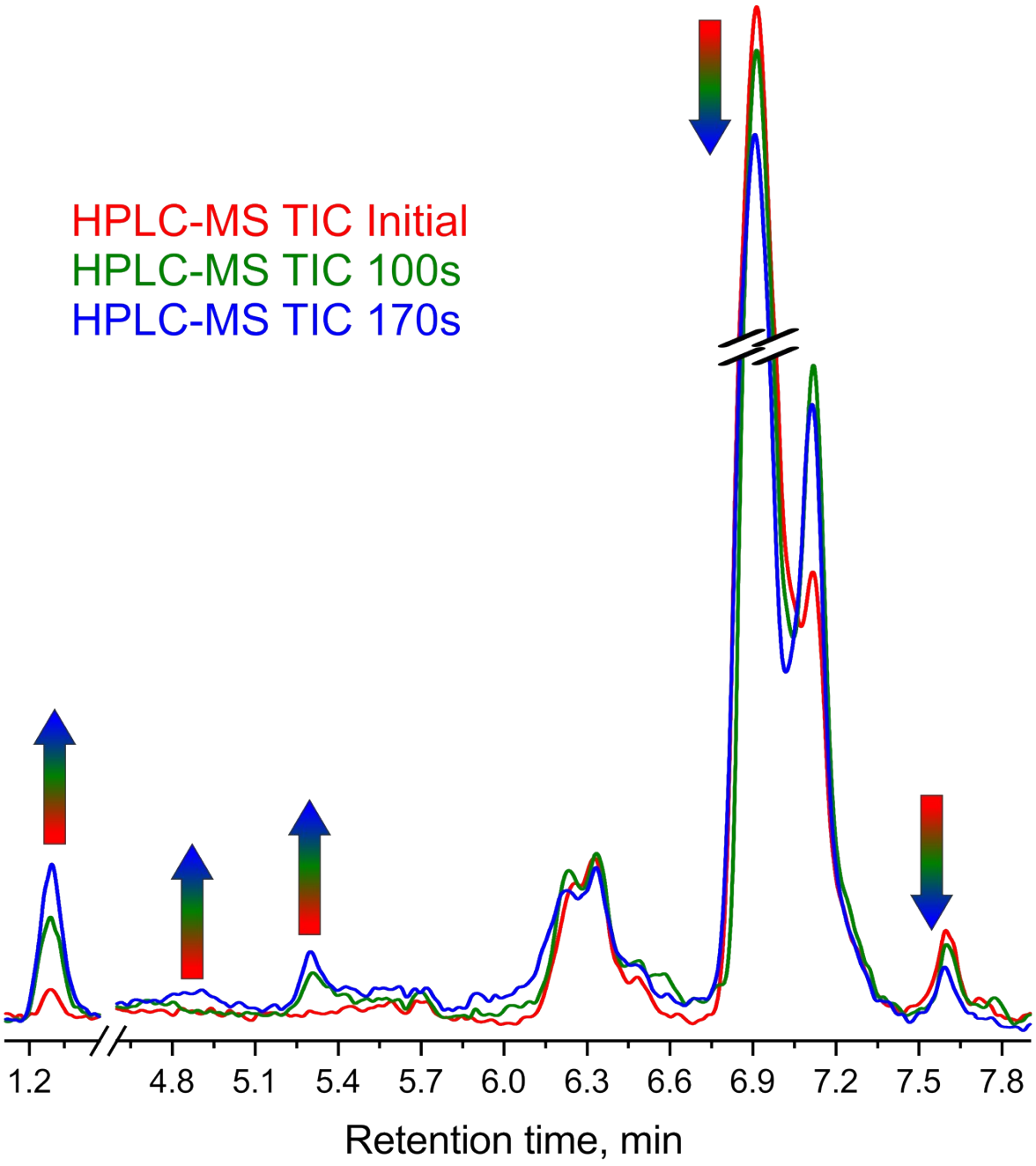

Figure S6-1. Chromatogramm of acetonitrile solution of [RuNO(β-Pic)$_2$(NO$_2$)$_2$OH] after irradiation.

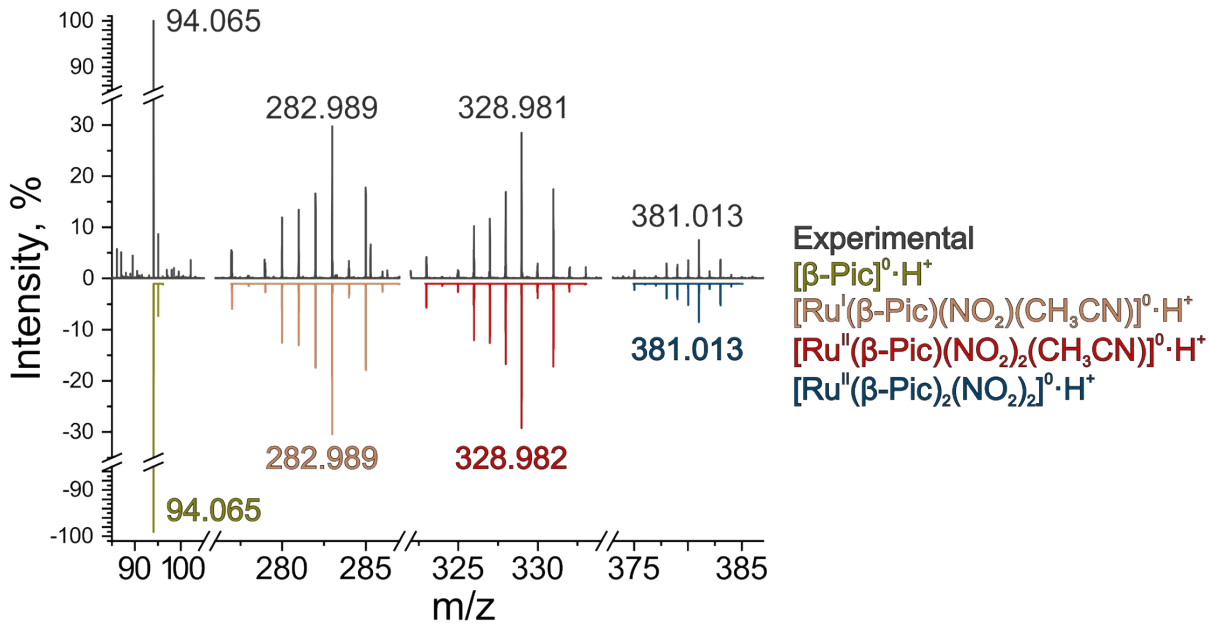

Figure S6-2.Mass spectra (experimental – over zero and calculated – below) of fraction with retention time 1.3 min.

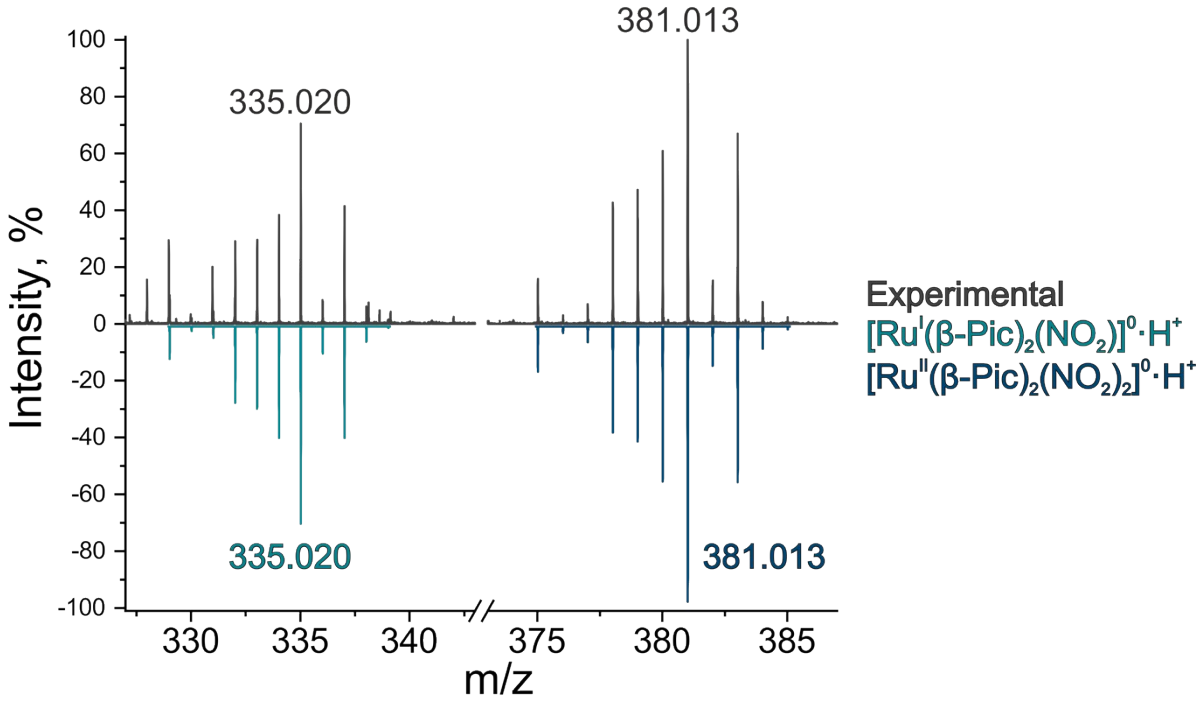

Figure S6-3.Mass spectra (experimental – over zero and calculated – below) of fraction with retention time 4.8-5.4 min.

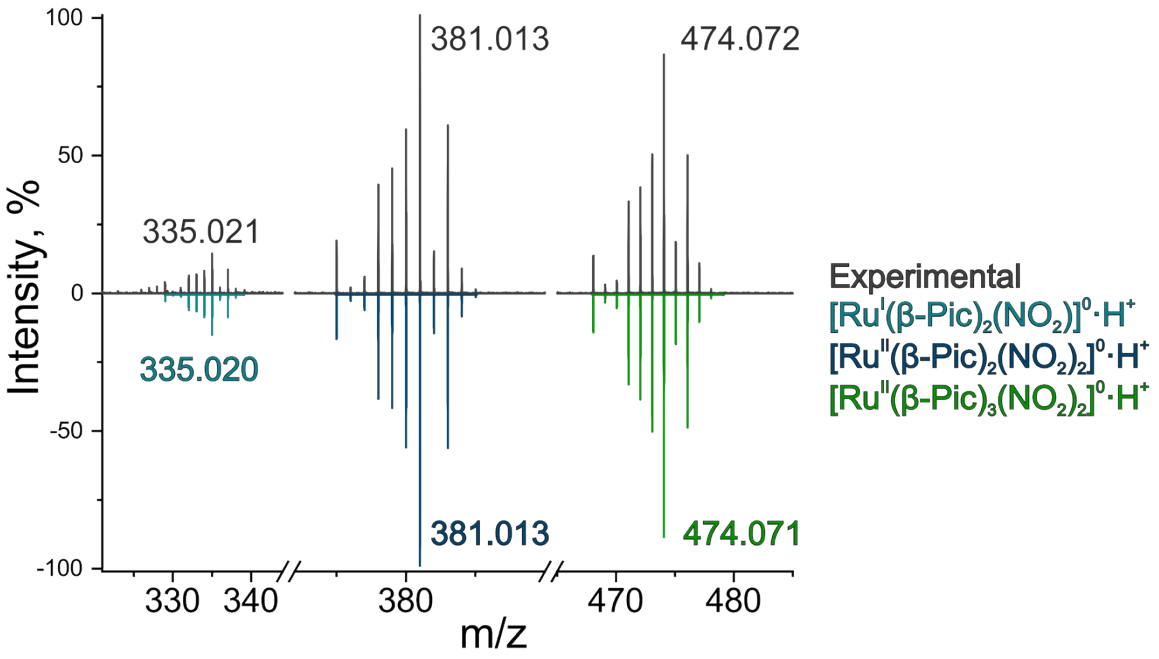

Figure S6-3.Mass spectra (experimental – over zero and calculated – below) of fraction with retention time 6.0-6.6 min.

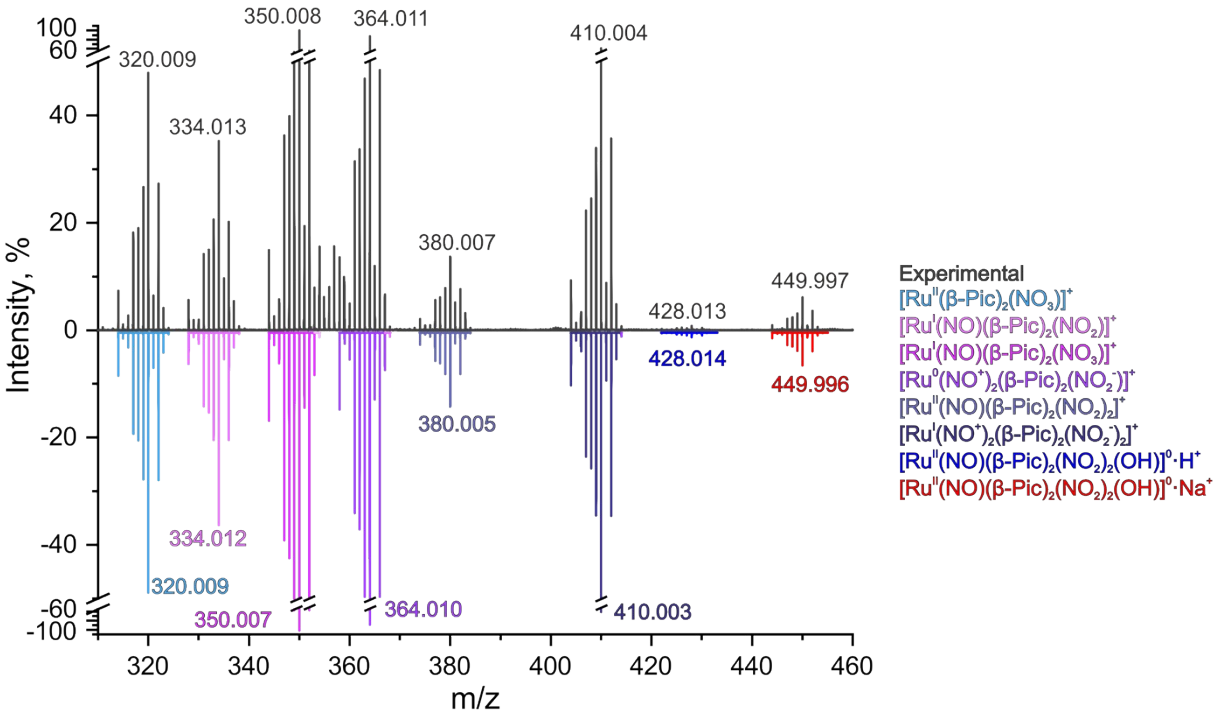

Figure S6-3.Mass spectra (experimental – over zero and calculated – below) of fraction with retention time 6.9-7.5 min.